Polycaprolactone–POSS Chemical/Physical Double Networks

Kyung Min Lee,[†] Pamela T. Knight,[†,‡] Taekwoong Chung,[†,‡] and Patrick T. Mather*[,‡,§]

Department of Macromolecular Science and Engineering, Case Western Reserve University, 2100 Adelbert Road, Cleveland, Ohio 44106, Syracuse Biomaterials Institute and Department of Biomedical and Chemical Engineering, Syracuse University, Syracuse, New York 13244

Received March 17, 2008; Revised Manuscript Received April 24, 2008

ABSTRACT: Biodegradable shape memory polymers are exciting materials, based on a combination of controlled degradation and triggered actuation that enables the design of unique medical devices. However, their synthesis requires precise control over thermomechanical properties often not possible with common building blocks for biodegradable polymers. In the present work, we report the preparation of "double networks" that feature a superposition of a covalent network with a percolative physical network, the latter being derived from a well-defined crystalline phase of strongly hydrophobic polyhedral oligosilsesquioxane (POSS) moieties. Each covalent network chain features polycaprolactone (PCL) tethers on a single POSS moiety by virtue of its use as a difunctional initiator for PCL ring-opening polymerization. Such network chains were synthesized to feature molecular weight values that ranged from 2000 to 4000 g/mol (polydispersity index <1.35) and POSS contents ranging from 49 to 24 wt %, respectively. Thermal analysis of the uncrosslinked network chains indicated competitive crystallization between POSS and PCL domains, with the PCL melting temperature (T_m) and percent crystallinity increasing with increasing PCL content in the diol, while the POSS T_m decreased, though always remaining higher than PCL. Covalent networks were prepared by end-capping the POSS–PCL telechelics with acrylate groups and photocrosslinking with stoichiometric addition of a tetrathiol cross-linker. Only those POSS-containing networks with high POSS loading, P-CL2-net (42 wt %) and P-CL2.5-net (34 wt %), showed evidence for POSS crystallization, while samples with lower POSS loading were dominated by PCL crystals that ostensibly prevented POSS crystallization. Dynamic mechanical analysis of P-CL2-net showed two rubbery plateaus, one between the glass transition temperature of PCL and the POSS melting point, and the other above the POSS melting point and extending to high temperatures. The first plateau, at a surprisingly high value of 150 MPa, was further investigated using rheometric crystallization studies on the diol precursor, P-CL2, which revealed a prominent sol–gel transition upon POSS crystallization during cooling. We reason that, in the cross-linked form, the same POSS crystal percolation yields a "double network", with a combination of both physical and chemical network junctions, as evidenced by two rubbery plateaus. The duel network structure enabled both one-way and two-way shape memory behavior, showing recoverable deformation (strain) and increased performance with repetitive cycling.

Introduction

Organic–inorganic hybrid materials receive significant attention from polymer scientists, inspired by remarkable potential to combine two dramatically different material classes at the molecular level. A goal of hybrid materials (a type of composite) has long been to combine the functionality and processibility of an organic phase with the heat/chemical stability and enhanced modulus of an inorganic phase. For polymer-based nanocomposites, numerous approaches have been elaborated, including in situ sol–gel chemistry,[1,2] organoclay intercalation and exfoliation,[3–5] and use of hybrid inorganic–organic monomers (macromers) such as polyhedral oligosilsesquioxane (POSS). Incorporation of POSS macromers within polymeric architectures allows the organic and inorganic phases to interact at the molecular level and with assured compatibilization. POSS itself is a hybrid material, being a well-defined spherosilicate polyhedral molecule with general composition $R'_1R_7Si_8O_{12}$ and possessing an inner cage diameter of approximately 0.5 nm.[6] For inorganic–organic compatibilization within a polymeric host, seven of the silicon vertices (R) are tethered with a short organic group (here isobutyl) while the eighth vertex (R') is tethered to a chemically reactive group (here diol). One advantage that POSS offers is chemical versatility, allowing it to be incorporated into many polymer matrices, such as polynorbornene,[7] poly(4-methylstyrene),[8] polymethacrylate,[9] ethene–propene copolymers,[10] siloxane polymers,[11] epoxides,[12] and dendrimers.[13] Overall, POSS-incorporated polymer nanocomposites show an increase in use temperature, oxidative resistance, and surface hardening.[14]

It is now well-known that POSS inherently aggregates to form nanocrystals. Zheng et al.[14,15]and Waddon et al.[15] synthesized copolymers containing ethylene and pendant POSS macromers. The POSS units were found to aggregate and form anisotropic crystalline structures, even when confined by the polymer backbone. Fu et al.[16,17] also proved this for POSS-containing polyurethane (PU) elastomers where POSS was sequestered in the hard segment and enhanced the microphase separation between hard and soft segments. Kim and Mather[18,19] reported the synthesis and characterization of amphiphilic telechelics where POSS was connected through urethane linkages to both ends of poly(ethylene glycol) (PEG) homopolymer chains. They observed modified crystallization behavior of the POSS–PEG–POSS telechelics due to the bulkiness of the POSS groups with respect to crystalline lamellae dimensions. Our present work exploits such crystallization by adopting a similarly well-defined architecture that is cross-linked to give a double network of chemical and physical junctions, as will be discussed later.

POSS incorporation into chemical networks has been explored previously with work focusing mainly on POSS aggregation as it relates to reactivity, solubility, and POSS–POSS interactions. Matejka, et al.[20] explored epoxide-functionalized POSS mol-

* Corresponding author. Email: ptmather@syr.edu.
† Department of Macromolecular Science and Engineering, Case Western Reserve University.
‡ Syracuse Biomaterials Institute, Syracuse University.
§ Department of Biomedical and Chemical Engineering, Syracuse University.

10.1021/ma800586b CCC: $40.75
Published on Web 06/13/2008

ecules for inclusion into a classic epoxy network. It was found that pendant, monoepoxy POSS molecules with phenyl and cyclopentyl functional groups were well dispersed within the network and could form crystallites whereas larger functional groups served to hinder aggregation and were found to be amorphous. Inclusion of octaepoxy POSS, used as a cross-link junction, did not disperse well in the matrix and homogeneity of the system only occurred after the network formation (i.e., reaction) had begun. A similar octaepoxyPOSS thermoset was investigated by Kim et al.,[21] who found that varying the cross-linking stoichiometry altered the POSS aggregation in the network and led to various nanomechanical deformation structures which enhanced toughness of the solid. Zucchi et al.[22] expanded on this work by investigating the role of nonreactive functional groups (R groups being isobutyl or phenyl substituents) on monoepoxy−POSS molecules as well as how prereacting the POSS with an amine small molecule before adding it to the epoxy network helped homogenization of the system. The isobutylepoxy−POSS was found to dissolve in the matrix both with and without prereaction. Phase separation occurred in both cases during network formation, but without the prereaction, the POSS was found to aggregate easily into smaller particles that crystallized upon cooling. The phenylepoxy−POSS system was much more complicated and led to amorphous POSS domains dispersed in the epoxy matrix. Contrary to the findings from Matejka, Bizet et al.[23] found that an octafunctionalized methacrylated POSS had good miscibility in a diacrylate small molecule matrix and phase separation was inhibited during the polymerization. In the case of a monofunctionalized epoxy-POSS, the POSS was initially miscible when a reactive diluent was used, but readily phase separated into nanoclusters and even prevented covalent inclusion into the network. The work presented herein is similar to the prereacted POSS scenario, but the extent of POSS aggregation is dictated by the length of two tethered PCL chains as well as the competitive crystallization between the two species in the network.

One area in which POSS has not been fully explored is its use in shape memory polymers (SMPs). SMPs are an exciting class of stimuli-responsive materials that can undergo dramatic shape changes based on specific environmental conditions.[24,25] Two broad classes of SMPs have been elaborated in the literature: one-way (1W-SMP) and two-way (2W-SMP). For 1W-SMPs, the sample is deformed into a temporary shape and "fixed" through cooling. The material can then spontaneously return to its original shape through subsequent heating. Jeon, et al.[26] reported the 1W-SM properties of norbornene-based random copolymers containing either cyclopentyl- or cyclohexyl-substituted POSS. Compared to pure polynorbornene, the POSS hybrids allowed for an increase in both retraction and high temperature stability, although a slight decrease in percent recovery did occur. On the other hand, 2W-SMPs[27,28] can switch between two permanent shapes through an elongation/retraction phenomenon that occurs under a constant applied force during cool/heat cycles. This phenomenon stems from network chain elongation during an ordering transition under load.

For the present work, we sought to prepare and study degradable shape memory polymeric networks with single POSS moieties located precisely in the middle of the network chains, hypothesizing that this regularity of placement would promote POSS crystallization even within a constraining network structure. Thus, we report herein on the successful synthesis of POSS-initiated polycaprolactone (PCL) telechelic diols, utilizing a POSS diol macromer as the difunctional initiator. PCL is a well-known biodegradable polymer. The POSS−PCL diols were then terminated with acrylate groups and photocured in the presence of a tetrathiol cross-linker. While PCL networks for biomedical applications have previously been pioneered and extensively explored by Lendlein et al.[29,30] and Bellin et al.,[31] showing excellent one-way[29,30] and even triple[31] shape memory properties, respectively, the current research offers a new class of materials with enhanced stiffness and versatility due to the POSS incorporation. The phase behavior, underlying microstructure, and thermomechanical behavior for these materials were studied with systematic variation in architectural parameters, revealing quite unique properties. Subsequent studies will focus on biodegradation properties and utilization as tissue engineering scaffolds.

Experimental Section

Materials. ϵ-Caprolactone monomer was vacuum-distilled and stored under nitrogen prior to use. Tin(II) 2-ethylhexanoate catalyst (Aldrich) was also kept under nitrogen. 2-ethyl-2-[3-[[(heptaisobutylpentacyclo-[9.5.1.1^{3,9}.1^{5,15}.1^{7,13}]octasiloxanyl)oxy]dimethylsilyl]-propoxy]methyl]-1,3-propanediol (or "TMP diolisobutyl-POSS"), hereafter referred to as POSS diol, was purchased from Hybrid Plastics as a pure (>99%) crystalline solid and used as received. Polycaprolactone (PCL) homopolymers having molecular weight (M_n) averages of 1250, 2000, and 3000 g/mol, benzene (anhydrous), triethylamine, acryloyl chloride, 2,2-dimethoxy-2-phenylacetophenone, and pentaerythritol tetrakis(3-mercaptopropionate) (hereafter, "tetrathiol") were purchased from Aldrich and used as received. All other solvents were purchased from Fisher Scientific and used without further purification.

Synthesis of POSS-Initiated Telechelic Diols, Macromers, and Networks. We followed methods outlined elsewhere for ring-opening polymerizations,[32,33] but applied it to our unique composition and architecture.

POSS Telechelic Diol. For example, to synthesize a POSS-initiated polycaprolactone diol with number-average molecular weight of 2500 g/mol (called P-CL2.5), 5 g (34.7 mmol) of purified ϵ-caprolactone, 3.63 g (3.45 mmol) of dried POSS diol, and ca. 15 mg of tin(II) 2-ethylhexanoate as catalyst were charged into a 100 mL flask under a nitrogen atmosphere, and the mixture was stirred at 140 °C for 24 h. The resulting telechelic diol was allowed to cool to room temperature, dissolved in tetrahydrofuran (THF), and then precipitated into *n*-hexanes, filtered, and dried. Several POSS-initiated PCL telechelics of varying molecular weights were synthesized, as illustrated in Scheme 1, with the amount of POSS diol involved in the synthesis ranging from 5.55 g (5.27 mmol) to 1.78 g (1.69 mmol). The synthetic yield for each of these reactions was typically over 95%. The samples are named using the convention P-CL*n*, where *n* indicates the total number-average molecular weight of the diol as prescribed by the feed molar ratio of POSS initiator to ϵ-caprolactone monomer and measured using ^{1}H NMR. Gel permeation chromatography (GPC) was also utilized in order to determine the polydispersity of each sample. ^{1}H NMR of P-CL2.5 ($CDCl_3$): 0.106 (s, 6H, $-Si-(CH_3)_2$), 0.607 (q, 14H, $-Si-CH_2-CH-$), 0.950 (q, 42H, $-CH-(CH_3)_2$), 1.39 (m, $-CH_2-CH_2-CH_2-$), 1.65 (m, $-CH_2-CH_2-O-$), 1.85 (m, 7H, $-CH-(CH_3)_2$), 2.31 (t, $-OOC-CH_2-CH_2-$), 3.34 (m, $-C-CH_2-OOC-$), 3.66 (t, $-CH_2-OH$), 4.06 (t, $-CH_2-CH_2-OOC-$). A typical ^{1}H NMR spectrum is given in the Supporting Information (Figure S1).

POSS−PCL Macromers. Each of the synthesized diols described above were end-capped to yield acrylated end groups. For this purpose, 1 mmol of each POSS−PCL telechelic diol was added to anhydrous benzene under a nitrogen atmosphere along with 2.3 mmol of triethylamine. While stirring, 2.3 mmol of acryloyl chloride was added very slowly to the solution. The reaction was then carried out at 80 °C for 3 h, filtered to remove the resulting triethylamine hydrochloride, and then precipitated in *n*-hexanes and dried under vacuum. The percent yield from the collected product averaged 85%. The extent of acrylate end-capping was determined by NMR and found to range from 85% to 93%. Samples thus converted to the acrylated form are referred to as P-CL*n*-mac. ^{1}H NMR of P-CL2.5-mac ($CDCl_3$): 0.106 (s, 6H, $-Si-(CH_3)_2$), 0.607 (q, 14H, $-Si-CH_2-CH-$), 0.950 (q, 42H, $-CH-(CH_3)_2$), 1.39 (m,

Scheme 1. Preparation of POSS-Initiated Polycaprolactone Diol, Macromer, and Photo-Cross-Linked Network

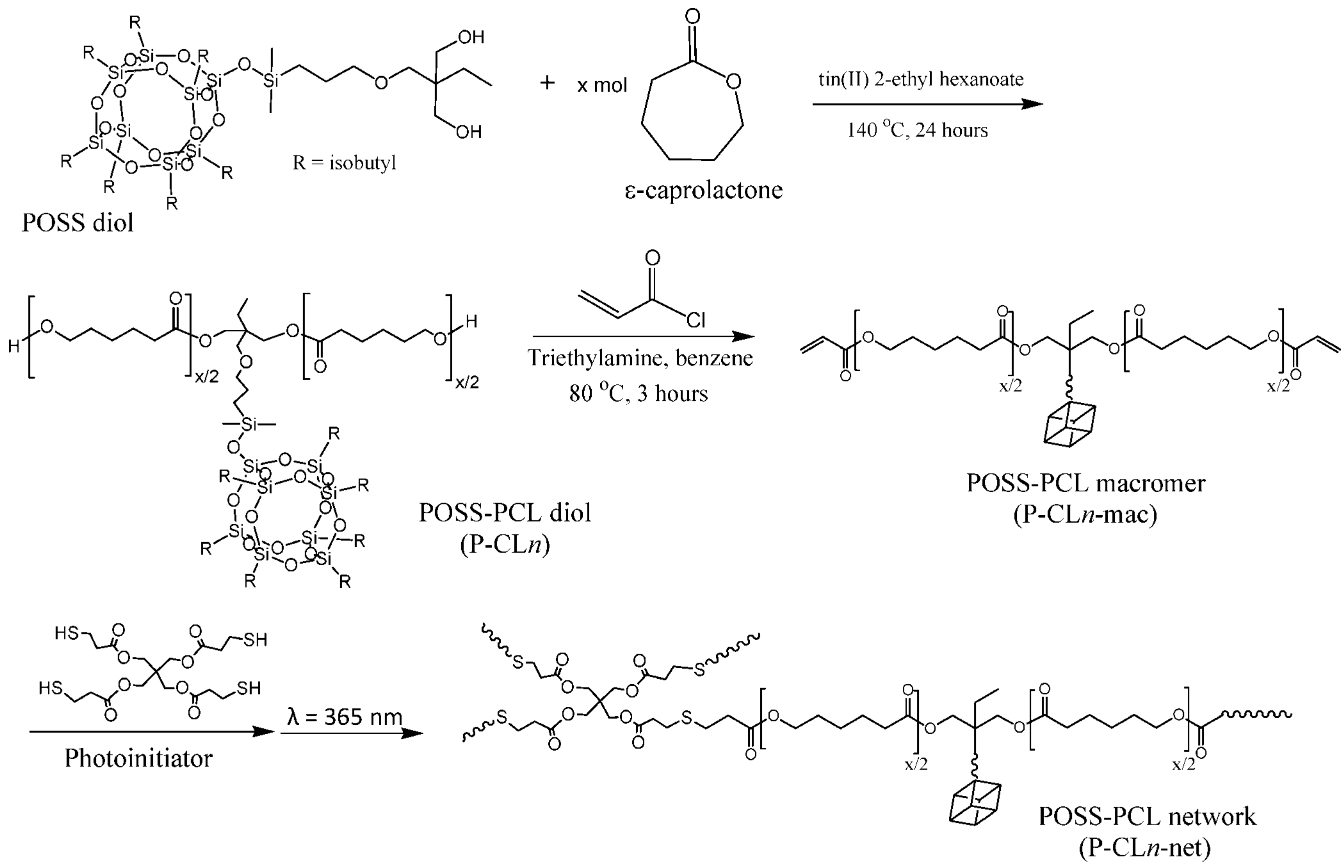

$-CH_2-CH_2-CH_2-$), 1.65 (m, $-CH_2-CH_2-O-$), 1.85 (m, 7H, $-CH-(CH_3)_2$), 2.31 (t, $-OOC-CH_2-CH_2-$), 3.34 (m, $-C-CH_2-OOC-$), 4.06 (t, $-CH_2-CH_2-OOC-$), 4.14 (t, $-CH_2-OOC-C{=}C$), 5.81 (dd, $COO-CH{=}CH1trans$), 6.1 (dd, $COO-CH{=}CH2cis$), 6.4 (dd, $COO-CH{=}CH_2$). A typical ^{1}H NMR spectrum is given in the Supporting Information (Figure S1).

POSS−PCL Networks. To prepare chemically cross-linked networks, POSS−PCL macromers were mixed with the tetrathiol cross-linker and a photoradical generator and then exposed to intense ultraviolet light. For example, P-CL2.5-net was prepared by first adding 0.5 g (1.77 mmol) of P-CL2.5-mac to a 20 mL scintillation vial and dissolving in 1 mL of dichloromethane. Next, 0.885 mmol of tetrathiol cross-linker (1:2 molar ratio of thiol to double bond functionality) and 2 wt % of photoradical generator (2,2-dimethoxy-2-phenylacetophenone) was added. The clear solution was then irradiated (5 cm above) with UV light (1200 μW/cm^2) at a wavelength of 365 nm at room temperature for 1 h. The network was purified with extraction by submerging it in warm dichloromethane (~40 °C) overnight and drying under vacuum at 50 °C prior to analysis. Gel content values were found to be 90%, on average. Network samples are referred to as P-CL*n*-net.

Molecular Characterization. To determine the chemical structure and molecular weight (M_n) of the POSS−PCL diols, ^{1}H NMR spectroscopy (Varian Inova spectrometer, 600 MHz, 128 scans) was performed at room temperature using deuterated chloroform as the solvent. Gel permeation chromatography (GPC) was conducted in HPLC-grade tetrahydrofuran (THF) using a Varian Pro Star system with a Viscotek dual detector attachment used for viscosity and light scattering measurements. Solutions were prepared from THF (~5 mg/mL) and passed through a 0.45 μm PTFE filter prior to injection. The GPC was operated at a flow rate of 1 mL/min and featured a series of three columns of cross-linked polystyrene beads. The first two columns were 5 and 30 cm long columns (Polymer Laboratories, Inc.), consecutively, each packed with 3 μm particles designed for separations of polymers with molecular weight less than 25,000 g/mol. The third column was a mixed-bed column (Tosoh Bioscience GMHHR-M) 30 cm long and featuring a 5 μm particle size affording separation of higher molecular weight polymers. Note that the average molecular weights for the telechelics synthesized were close to the lower limit of accuracy for the columns (<5000 g/mol). Therefore, only polydispersity values for these POSS−PCL diols were used from GPC measurement. Molecular weights were obtained from ^{1}H NMR using the POSS molecule as an internal standard, as will be discussed later.

Thermal Analysis. The glass transition temperatures (T_g), melting temperatures (T_m), and latent heats of fusion (ΔH) were determined using differential scanning calorimetry (DSC, TA Instruments Q100 equipped with a refrigerated cooling accessory) under a nitrogen purge. As a reproducible thermal history, the POSS−PCL diols, macromers, and networks were heated to 200 °C, then cooled to −90 °C at a rate of 10 °C/min and heated once more to 200 °C using the same rate. The PCL homopolymers underwent the same heat/cool cycles, but only up to 100 °C due to thermal stability constraints. Values reported for T_g, T_m, and ΔH are taken from the second heating traces.

Dynamic Mechanical Analysis and Shape Memory Characterization. Linear viscoelastic thermo-mechanical properties of the materials were determined using dynamic mechanical analysis (DMA). A TA Instruments Q800 apparatus was employed in tensile mode with a preload force of 10 mN, an oscillation amplitude of 5 μm (<0.18%), static stress/dynamic stress amplitude ratio ("force tracking") of 125%, and an oscillation frequency of 1 Hz. Samples were cut from the cured networks to feature dimensions of 10 mm (length) × 1.6 mm (width) × 0.8 mm (thickness). After loading each film specimen at room temperature under tensile stress, they were cooled to $T = -70$ °C, thermally equilibrated, and finally ramped to 130 °C at a rate of 3 °C/min. The same size samples were used for shape memory cycles. For 1W-SM, samples (in tension) were equilibrated at 110 °C, elongated to a force of 0.23 N at a rate of 0.025 N/min, cooled to 30 °C at a rate of 2 °C/min, unloaded to 0.005 N using the same rate as before, then heated to

Table 1. Molecular Characteristics and DSC Results of POSS−PCL Diols, Macromers, and Cross-Linked Networks

sample name	M_n (g/mol)	POSS content (wt %)	$T_{g,PCL}$[d] (°C)	$T_{m,PCL}$[d] (°C) [ΔH (J/g)]	$T_{m,POSS}$[d] (°C) [ΔH (J/g)]
P-CL2	2130[a]	49[a]	−64.8	−11.0 [1.74]	91.5 [11.90]
P-CL2-mac	2240[b]	47[b]	−66.2	−12.3 [1.25]	78.7 [9.20]
P-CL2-net		42[c]	−48.2		85.7 [7.65]
P-CL2.5	2720[a]	39[a]	−67.2	16.8 [12.3]	81.1 [6.95]
P-CL2.5-mac	2830[b]	37[b]	−67.7	31.8 [14.5]	68.2 [3.01]
P-CL2.5-net		34[c]	−54.8		66.8 [3.90]
P-CL2.75	2900[a]	36[a]	−66.9	22.9 [31.9]	79.3 [5.79]
P-CL2.75-mac	3010[b]	35[b]	−60.8	48.1 [46.8]	60.1 [0.10]
P-CL2.75-net		32[c]	−51.0	38.9 [33.8]	
P-CL3	3550[a]	30[a]		45.4 [46.8]	68.8 [1.80]
P-CL3-mac	3660[b]	29[b]		46.8, 51.9 [59.3]	
P-CL3-net		27[c]	−51.0	42.7 [36.1]	
P-CL4	4450[a]	24[a]		48.7, 53.1 [64.7]	
P-CL4-mac	4560[b]	23[b]		48.1, 53.2 [56.6]	
P-CL4-net		22[c]	−50.2	46.9 [45.8]	

[a] Determined from ^{1}H NMR. [b] Calculated values based on each acrylate end group having molar mass 55 g/mol. [c] Calculated values based on the mole ratio of macromer to cross-linker being 2:1 and the tetrathiol having MW = 489 g/mol. [d] Determined from DSC second heating traces.

110 °C at a ramp rate of 2 °C/min. This process was then repeated two more times on the same sample in order to obtain multiple cycles. For 2W-SM, the cycling was much the same as for 1W-SM, except that a substantial applied force was maintained throughout the entire shape memory cycle.[24]

Wide Angle X-ray Diffraction (WAXD). To determine the underlying microstructure of our samples, WAXD experiments were performed on both the POSS−PCL diols and networks using a Rigaku MSC D/Max Ultima X-ray diffractometer with a Cu Kα source (λ = 1.54 Å) at ambient temperature. Scans were run from a 2θ value of 2.5 to 40° at a scan speed of 0.4°/min.

Optical Microscopy (OM). An optical microscope (Olympus BX50 microscope) and a composite color CCD camera (Panasonic GP-KR222) were used to observe the POSS aggregation in POSS−PCL telechelics. For this, the desired POSS−PCL diol was dissolved in dichloromethane (2 wt %) and 2 drops of the solution were placed onto a glass slide. The sample was then dried under vacuum at 45 °C overnight before obtaining micrographs.

Linear Viscoelastic Shear Measurements. POSS aggregation in the POSS−PCL telechelics upon cooling was also quantified using linear viscoelastic shear measurements as recorded by an Anton Paar rheometer (Physica MCR 501). Measurements were carried out using parallel disk geometry with a diameter of 25 mm, angular frequency of 0.05 rad/s, and sample thickness ranging from 0.5 mm to 1 mm. Samples were heated to fluidity at 110 °C, held for 5 min, and then cooled down to a crystallization temperature of 89 °C using a ramp rate of 1 °C/min and held for an additional 15 min. The storage modulus of the sample with time was recorded once the cooling began, revealing the impact of crystallization on macroscopic linear viscoelastic properties.

Results and Discussion

Synthesis and Characterization of POSS-Initiated PCL Telechelics. A series of POSS−PCL telechelic diols with various PCL lengths was synthesized using POSS diol as the difunctional initiator to ring-open ϵ-caprolactone monomers in the presence of tin(II) 2-ethylhexanoate as a catalyst. The total target molecular weight of the POSS−PCL telechelics (M_n = 2000, 2500, 2750, 3000, and 4000 g/mol) was specified by the molar ratio of ϵ-caprolactone to POSS diol, thus controlling the length of each of the two PCL tethers grafted from the two reactive sites of the POSS (M_{POSS} = 1052 g/mol). The actual M_n obtained was then determined by ^{1}H NMR (trace shown in the Supporting Information, Figure S1) using POSS as the internal standard. Specifically, the integral of the POSS peak at 0.1 ppm was set to denote six protons (two methyl groups pendant to a silicon, peak "a" in Figure S1). Since there is one POSS molecule per polymer chain, integrating over the PCL peak at 2.3 ppm (methylene protons next to the carbonyl of the ester group, peak "d" in Figure S1) and dividing by two (for two protons) gives the number of caprolactone repeat units. Multiplying this number of repeat units by the molecular weight of the CL repeat unit (144 g/mol) and adding the molecular weight of POSS (1052 g/mol) gives the final number-average molecular weight of each diol, as shown in Table 1. Values obtained were within 10% of the target molecular weight for P-CL2, P-CL2.5, and P-CL2.75, indicating good synthetic control. The M_n for the diols P-CL3 and P-CL4 were slightly larger than expected by 19% and 12%, respectively; however, each still displayed a narrow, monomodal distribution of molecular weights, discussed below. The weight percent of POSS present in the as-synthesized diols ranged from 49 wt % to 24 wt %. Molecular characteristics for these materials after each step of the synthesis are summarized in Table 1.

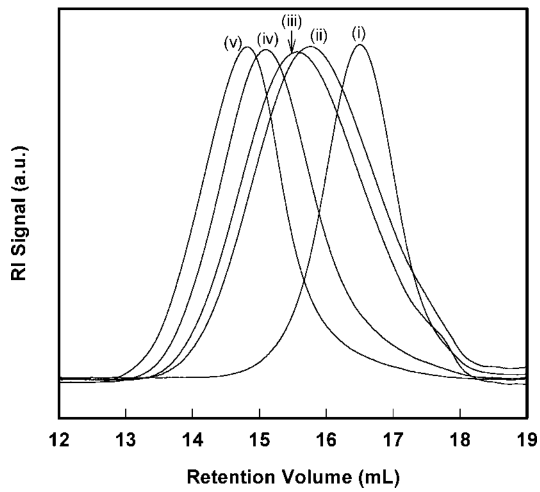

Figure 1. Gel permeation chromatography (GPC) curves for (i) P-CL2, (ii) P-CL2.5, (iii) P-CL2.75, (iv) P-CL3, and (v) P-CL4 telechelic diols.

GPC results, shown in Figure 1, for the POSS−PCL telechelics reveal relatively narrow polydispersity indices (PDI), with M_w/M_n ranging from 1.10 to 1.35, and symmetric, unimodal curves. Molecular weights determined by GPC analysis for the POSS−PCL diols were uniformly higher than those obtained by ^{1}H NMR spectroscopy, although the peak elution volumes followed the same ranking. Only the polydispersity index (PDI) and relative peak elution order (higher M_n eluting first) were considered further.

DSC first cooling and second heating scans for the POSS−PCL telechelic diols are shown in Figure 2. All five POSS−PCL telechelics showed a melting transition from the PCL tethers, although the melting for P-CL2 (∼50 wt % POSS) is only

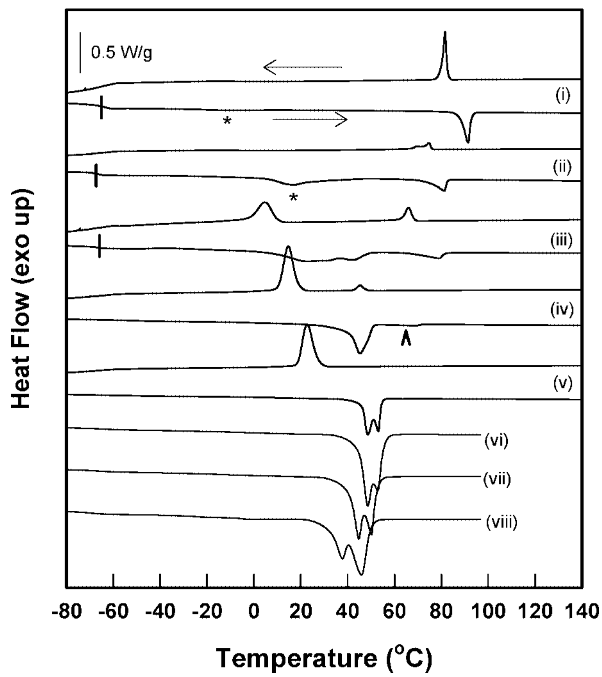

Figure 2. DSC traces showing first cool and second heating traces for the (i) P-CL2, (ii) P-CL2.5, (iii) P-CL2.75, (iv) P-CL3, and (v) P-CL4 diols and second heatings only for corresponding PCL homopolymers with M_n of (vi) 3000 g/mol, (vii) 2000 g/mol, and (viii) 1250 g/mol. Dashes are used to highlight T_g from the CL tethers while the stars and arrowhead point out CL and POSS melting, respectively, that were observed after zooming in on the plot.

visible upon significant scale expansion (denoted by a star in Figure 2, trace i). Melting from POSS-based crystalline aggregates was evident at comparatively higher temperatures (65 °C > $T_{m,POSS}$ > 95 °C) in each of the samples except P-CL4 where POSS makes up less than 25% of the total weight. The PCL melting temperature ($T_{m,PCL}$) and heat of fusion of PCL ($\Delta H_{m,PCL}$) increased with increasing PCL content, whereas POSS melting temperature ($T_{m,POSS}$) and heat of fusion ($\Delta H_{m-,POSS}$) decreased. Correcting for the weight of PCL in the diols and considering the heat of fusion for pure PCL is 126 J/g,[34] the crystallinity of the PCL component in P-CL2, P-CL2.5, P-CL2.75, P-CL3, and P-CL4 was calculated to be approximately 3%, 16%, 40%, 52%, and 67%, respectively.

The observed trends suggest that the crystal formation of one component (POSS or PCL) hinders the other, resulting in imperfect crystal structures for both components.[14,18] Similar results were observed by Kim and Mather[18,19] who reported that covalently end-capping poly(ethylene oxide) (PEO) with POSS macromers disrupted the crystallization of PEO, resulting in less ordered crystals and subsequently lower melting temperatures and heats of fusion. For comparison purposes, the second heating traces for three PCL homopolymers with molecular weights similar to those of the PCL component in the telechelics (M_n = 1,250 g/mol, 2,000 g/mol, and 3,000 g/mol) are also shown in Figure 2, although these samples were only heated to 100 °C. The homopolymers exhibit a double melting transition that may indicate a sequence of melting/recrystallizing/melting possible in systems with significant secondary crystallization.[35] The melting temperature increased with increasing molecular weight of PCL, and crystallinity of the PCL homopolymers was calculated to be 57%, 61%, and 63%, respectively. This type of double melting upon heating was observed only for the telechelic with the highest weight percent PCL, P-CL4, probably also due to a melting/recrystallization/melting sequence. With only 23 wt % POSS, the CL tethers of P-CL4 have more freedom to crystallize in a favorable manner, such as it would if POSS was not present. Subsequently, the melting peaks for P-CL4 occur in the same region as the PCL homopolymer with M_n of 3000 g/mol.

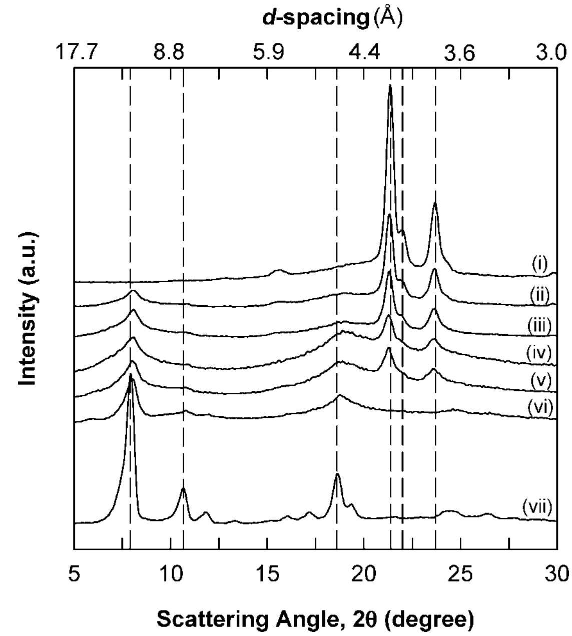

Figure 3. Wide angle X-ray diffraction patterns for (i) pure PCL homopolymer with a molecular weight of 3000 g/mol, the POSS−PCL telechelic diols (ii) P-CL4, (iii) P-CL3, (iv) P-CL2.75, (v) P-CL2.5, (vi) P-CL2, and (vii) pure POSS diol.

The POSS-containing telechelics, as well as POSS monomer and PCL homopolymers, were further analyzed for their microstructure using wide-angle X-ray diffraction (WAXD) and the associated diffractograms are shown in Figure 3. The pure POSS diol (TMP diolisobutyl−POSS) exhibits strong reflections at 2θ values of 7.9° (11.2 Å), 10.62° (8.3 Å), and 18.6° (4.8 Å), suggestive of a rhombohedral[36] (or equivalently hexagonal crystal[6]) unit cell and nearly identical to the pattern for a propylmethacrylate-functionalized iBu−POSS studied by Kopesky and co-workers.[37] The relatively broad and small number of peaks prevented accurate peak indexing. The WAXD patterns of the PCL homopolymer with molecular weight of 3,000 g/mol shows strong diffraction peaks at 2θ = 21.4°, 22.0°, and 23.7°, corresponding to (110), (111), and (200) reflections.[38] These reflection peaks of the homopolymer agree with the reported unit cell parameters of PCL; that is, an orthorhombic unit cell with a = 7.47 Å, b = 4.98 Å. and c = 17.26 Å.[39] Most of the POSS−PCL diols exhibited virtually the same large diffraction peaks as those of the PCL homopolymers, although the shoulder-peak appearing at a 2θ value of 22.0° diminishes with increasing POSS content. For P-CL2, with 49 wt % POSS, CL diffraction peaks are not visible, but strong POSS reflections are evident. These diffraction peaks, at 2θ values around 8° and 18.8°, indicate a crystalline POSS phase for each of the telechelics.

Interestingly, P-CL4 also exhibits both reflection peaks from POSS and PCL crystalline phases despite the absence of any POSS melting endotherm in DSC. Considering the different thermal histories of these two samples, however, it is not surprising that a difference in microstructure might result, as we now explain. WAXD diffraction patterns were obtained from the as-precipitated diols which were dried at 50 °C, allowing POSS mobilization and possible crystal formation. Any initial POSS crystallinity of P-CL4 would be lost in DSC during the initial melting at 200 °C. For each of the diols, the WAXD pattern shows reflection peak positions for POSS crystalline aggregates and a crystalline PCL phase within 0.3° of the same peaks for the crystalline phase of each pure material, indicating

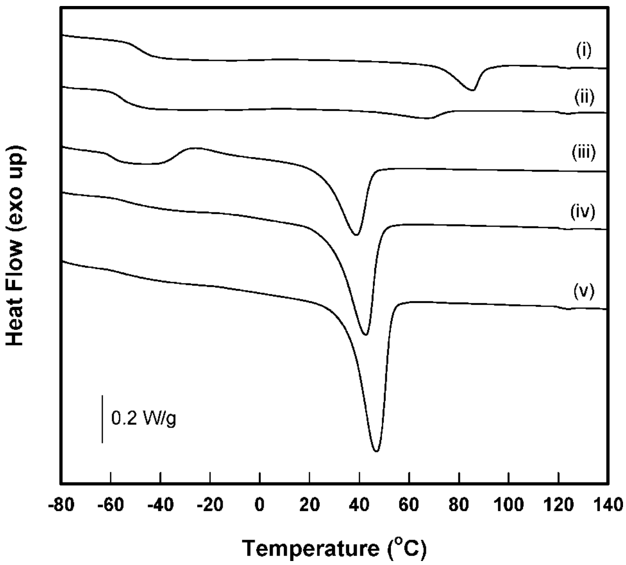

Figure 4. DSC second heating traces for the POSS−PCL networks (i) P-CL2-net, (ii) P-CL2.5-net, (iii) P-CL2.75-net, (iv) P-CL3-net, and (v) P-CL4-net.

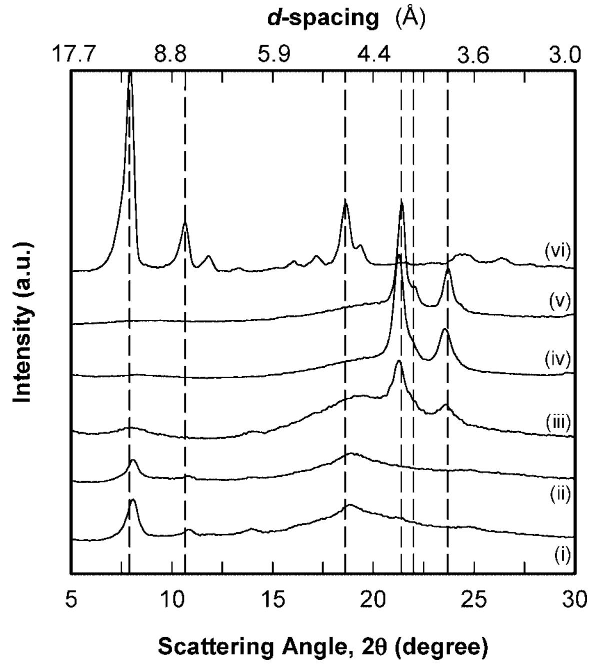

Figure 5. Wide angle X-ray patterns for (i) P-CL2-net, (ii) P-CL2.5-net, (iii) P-CL2.75-net (iv) P-CL3-net, (v) P-CL4-net, and (vi) pure POSS diol.

that the POSS core in the POSS−PCL telechelics did not alter the crystal structure of PCL, and vise versa. Here, we tentatively conclude that the POSS−PCL telechelics show a microphase-separated morphology at room temperature, and composition plays the decisive role in determining the final dominant phase (POSS vs PCL).

These results stand in contrast to our earlier findings,[40] where we reported that random copolymers of polystyrene and polystyrene-POSS featured molecular level POSS dispersion with WAXD results revealing no crystalline reflection peaks, even for POSS contents as high as 50 wt %. Random copolymerization in this system effectively prevented crystallization of POSS molecules. Considering those results and the present ones, we can conclude that polymer architecture is an important factor controlling POSS dispersion and crystallization. These findings will become important later on when looking into the rheological behavior of the POSS−PCL telechelics.

Synthesis and Characterization of POSS−PCL Networks. In order to prepare polymeric networks from the POSS-initiated PCL telechelics described above, the same compounds were terminated with acrylate groups (called POSS−PCL macromers) and photocured into networks using a tetrathiol cross-linker, as shown in Scheme 1. Although the acrylated polymers themselves can undergo cross-linking by UV irradiation, the use of a thiol cross-linker for ene-based systems has become prevalent due to advantages such as oxygen insensitivity and mobility of the thiyl radical.[41,42] Figure 4 exhibits the second heating DSC scans for each of the networks, with properties extracted being given in Table 1. All POSS−PCL networks show a T_g for the PCL component in the network near −50 °C indicating that the glass transition is not dependent on the amount of POSS in the system. On the other hand, the observed T_g is higher than that of the original telechelics and the pure PCL homopolymer (−60 °C), possibly due to constraints from the cross-linking. For P-CL2-net and P-CL2.5-net (42 and 34 wt % POSS, respectively), a modest melting endotherm was observed at a temperature above 60 °C, a value exceeding that for PCL, suggesting that it is associated with a crystalline POSS phase. The rest of the networks (<35 wt % POSS) exhibited strong melting peaks around 40 °C associated with PCL crystals.

To confirm these interpretations of the transitions observed with DSC, WAXD was run on each as-cured film and the diffractograms are shown in Figure 5. As expected, P-CL2-net and P-CL2.5-net show only POSS reflection peaks and no PCL crystalline peaks, whereas P-CL3-net and P-CL4-net show strong PCL reflection peaks and very small or no POSS reflection peaks. Only P-CL2.75-net exhibits reflection peaks from both POSS and PCL crystalline phases although the DSC trace only showed PCL melting. Indeed the low angle POSS peaks for P-CL2.75-net (Figure 5, trace iii) are too weak and diffuse to be considered crystalline. These diffraction results are consistent with the DSC thermograms for the POSS−PCL networks, but also suggest that POSS aggregation still occurs in the P-CL2.75-net sample.

POSS−PCL Double Networks. Figure 6 gives the tensile storage modulus, loss modulus, and tan(δ) data for P-CL2-net, the network containing the highest concentration of POSS (42%), along with the associated DSC trace for comparison. The sample shows two thermal transitions: a glass transition from the PCL chemically cross-linked network and a melting transition from the POSS physical network (crystalline regions), resulting in two rubbery plateaus, as we now explain. Focusing on the tensile storage modulus, the network is glassy at low temperatures ($T < T_g$) with an elastic modulus initially over 1 GPa. This value drops to ∼150 MPa as the PCL T_g is traversed and those chain segments become mobile. This plateau is then maintained over a very broad temperature range spanning 75 °C, until a sharp drop in modulus of roughly 2 orders of magnitude is observed near 90 °C due to POSS crystals melting. The flatness of the sub-T_m storage modulus is *quite unusual for semicrystalline networks*, which normally show continuous decay in modulus as the melting point is approached. Wide-angle X-ray diffraction and DSC studies for this same material indicate that the larger (lower temperature) rubbery plateau is associated with a POSS crystal network since no PCL crystal reflections or melting was observed and considering the modulus value >100 MPa.

The dynamic mechanical behavior of the POSS−PCL networks was found to depend strongly on composition, as shown in Figure 7. Inspecting the DMA traces for the series of POSS−PCL networks synthesized, it is apparent that the lower temperature, POSS-based, plateau becomes diminished and

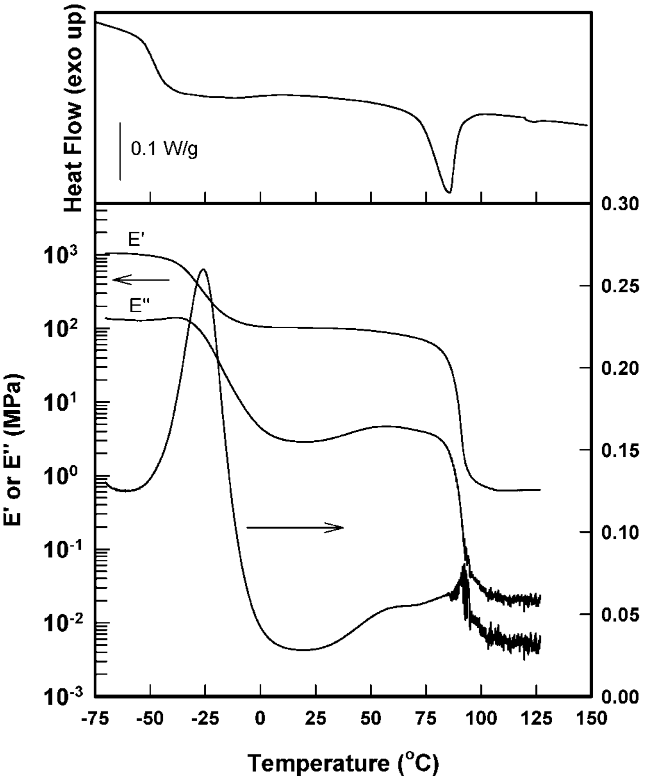

Figure 6. Tensile dynamic mechanical analysis (DMA) of P-CL2-net, measured using an oscillation frequency of 1 Hz. For comparison, the second heating trace from differential scanning calorimetry (DSC) of the same materials is shown (top).

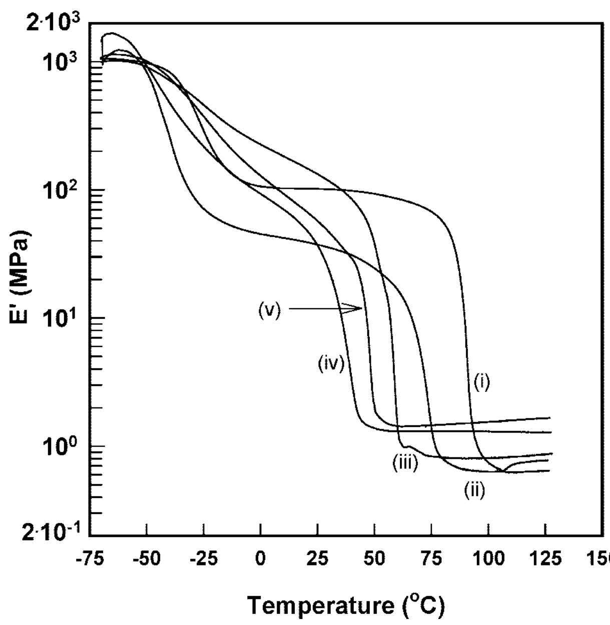

Figure 7. Tensile storage modulus (E') for all POSS−PCL networks: (i) P-CL2-net, (ii) P-CL2.5-net, (iii) P-CL2.75-net, (iv) P-CL3-net, and (v) P-CL4-net.

eventually disappears as the PCL weight percent in the network increases and POSS crystallinity is suppressed. In the absence of POSS crystallinity, the DMA traces adopt a form common to semicrystalline networks with a strongly sloped tensile storage modulus between the PCL T_g and T_m transition. The unique modulus flatness of the P-CL2-net system is clearly visible when compared, for example, to P-CL4-net. For only one sample—P-CL2.75-net—we observed thermomechanical evidence for both PCL and POSS melting, as anticipated for based on DSC and

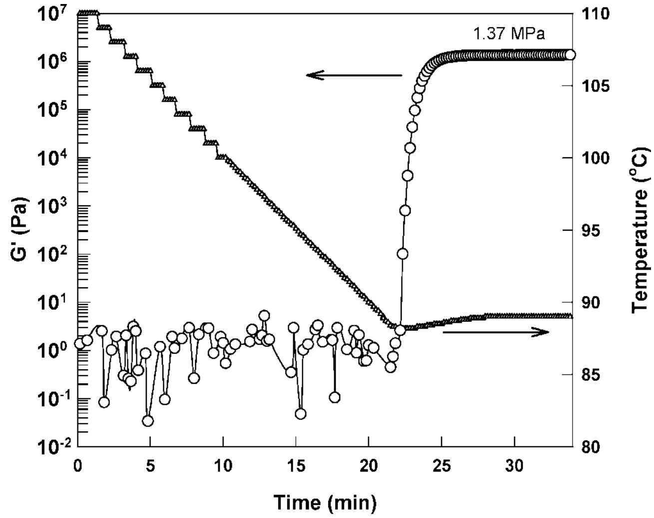

Figure 8. Crystallization of P-CL2 diol as monitored by linear viscoelastic measurements at a temperature of 89 °C. The sample was first heated to 110 °C (isotropic state), cooled at 1 °C/min down to the crystallization temperature, and then G' was measured with time at a frequency of 0.05 rad/s.

WAXD analyses. Close inspection of trace iii of Figure 7 in the region 45−60 °C (see Supporting Information for an expanded scale) reveals two softening points, which can be attributed to first POSS and then PCL melting. This takes into account the DSC data of Figure 4. Such an interpretation further explains the substantially higher modulus at room temperature for P-CL-2.75-net when compared to P-CL2.5-net and is consistent with the POSS crystallinity observed for P-CL2.75-net observed using WAXD.

At high temperatures - above any PCL or POSS melting temperatures - the tensile storage modulus surprisingly *increased* as the macromer molecular weight increased. This trend is opposite what one would expect from rubber elasticity theory ($E' \sim \rho RT/M_c$; where ρ is the density, R is the universal gas constant, T is the absolute temperature, and M_c is the molecular weight of each network strand) if we assume that each macromer is end-linked to a cross-link junction with a functionality of four as our polymerization chemistry would allow. Thus, it is apparent that increasing the POSS weight percent in a macromer (from P-CL4-mac to P-CL2-mac), decreases the cross-link density. This may be due to steric crowding by POSS or decreased macromer diffusivity.

In order to further investigate the surprisingly high modulus of the POSS-based plateau for P-CL2-net, crystallization experiments were performed on the precursor, P-CL2 diol, as shown in Figure 8. The sample was heated to a molten liquid state at 110 °C (consider DSC trace, shown in Figure 2, trace i) and held for 5 min before cooling down to 89 °C (slightly below melting transition seen in DMA for P-CL2-net) at 1 °C/min. The evolution of shear storage modulus was observed with time, anticipating the possibility of POSS aggregation. Initially, the sample is in a molten state, but the shear storage modulus increases dramatically once the crystallization begins, climbing to a large value of 1.37 MPa at equilibrium. However, the crystallization temperature chosen was found to be an important variable that determines the modulus change. Repeating the above experiment just one degree higher (90 °C) for the equilibrium temperature led to no crystal formation (molten liquid throughout) and one degree lower (88 °C) led to an even higher increase in modulus to 1.98 MPa (results not shown).

In either case, once crystallization occurs, the relatively high modulus achieved indicates that POSS crystals have percolated throughout the system, as opposed to existing as discrete

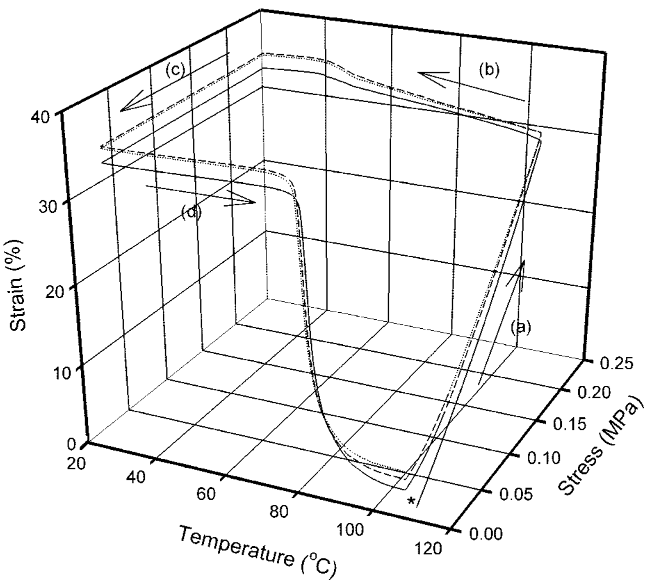

Figure 9. One-way shape memory cycles for P-CL2-net. Three cycles are shown: (—) first cycle, (- -) second cycle, and (• •) third cycle. The asterisk marks the beginning of the cycle and the arrows denote the various stages, specifically (a) deformation, (b) cooling/fixing, (c) unloading, and (d) recovery.

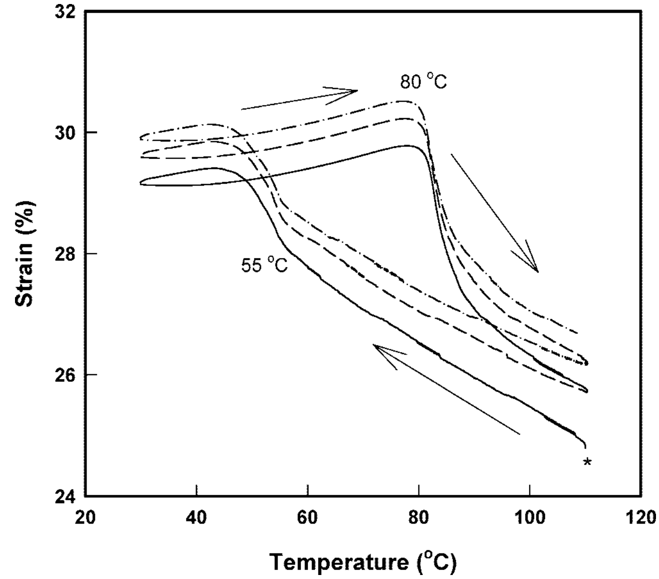

Figure 10. Two-way shape memory cycles for P-CL2-net. Three cycles are shown: (—) first cycle, (- -) second cycle, and (-•-) third cycle. The experiments begins at the asterisk with the sample being cooled, inducing rapid elongation at 55 °C. The sample was then heated and recovered to its original strain value after passing 80°.

domains, to create a POSS-based physical network among the amorphous PCL chains. In light of this finding, it can be inferred that upon cross-linking the P-CL2 diol (P-CL2-net), the film adopts a double-network structure with one network consisting of covalently linked PCL chains and the other physical from percolation of POSS crystalline aggregates. Furthermore, considering that POSS makes up slightly less than 50 wt % of the material, this percolation phenomenon also suggested to us that the POSS crystals exist in an extended form, either rodlike or layerlike, but not discrete as a spherical configuration would be.

While direct observations with TEM or AFM will be required to check for such morphological features (research that we have planned), we have been able to find evidence for propensity toward rodlike POSS aggregates during crystallization of the P-CL2 precursor telechelic. Thus, shown in Supporting Information is an optical micrograph of a thin film of P-CL2 prepared by casting from dilute solution at room temperature and revealing both spherical and rodlike POSS crystalline aggregates, along with a proposed mechanism for their formation. We present this mechanism as a suggested route in which the POSS network could develop, although further morphological studies of the P-CL2-net sample are necessary.

Shape Memory Behavior of POSS−PCL Networks. Utilizing the POSS crystallization discussed above for strain fixing, shape memory cycles were performed. Although the one-way and two-way SM behaviors of semicrystalline polymers having chain-folded crystallization, such as poly(cyclooctene), poly(ethylene glycol), polycaprolactone homopolymer, and multiblock polyurethane, have been reported, SM behavior using POSS crystallization for strain fixing has not been reported. Figure 9 shows a sequence of three one-way shape memory cycles for the P-CL-net through the POSS melting transition temperature. Similar findings were observed for P-CL2.5-net, but we focus here on P-CL2-net. After heating the film to 110 °C, deformation (a) was achieved by ramping to a load of 0.23 N. The sample was then cooled/fixed under this load (b) to 30 °C, during which period POSS crystallization occurs according to DSC (Figure 2, trace i). Next, the sample was unloaded (c) and subsequently heated/recovered (d) to 110 °C. Good shape fixing was observed since the sample did not retract (<0.5% decrease in strain for each cycle) upon removal of the deforming force at 30 °C. Recovery was also found to be almost 100% for each of the cycles, improving from 97.7% during the first cycle to 99% on the third cycle. Another point of interest is the slight increase in strain observed upon cooling at a temperature consistent with POSS crystallization (Figure 2). In light of our recent report of two-way shape memory behavior for semicrystalline polycyclooctene networks,[28] this finding of slight elongation during crystallization suggested a similar possibility for the present materials, although the underlying microstructural rearrangement responsible for the elongation event is unclear. Nevertheless, we proceeded with two-way shape memory testing.

Two-way, reversible, shape memory is a phenomenon that consists of cooling-induced elongation and heating induced contraction under a condition of constant applied mechanical load. Thus, for the 2W-SM cycles shown in Figure 10, the thermal treatment is similar to the 1W-SM, but there is no unloading step, and the actuation is derived from the material elongation/contraction during the cool/heat cycles. The tensile strains reported in the graph are the *total* strains, meaning the strain from the initial force at elevated temperature was not subtracted. As temperature decreases, the strain is observed to climb slowly then quickly increase the last few percent after cooling past 55 °C, correlating with the crystallization of POSS moieties. Upon heating, recovery begins only after 80 °C, near the melting temperature for POSS in unloaded P-CL2-net. After the contraction event of the first cycle, 99% of the strain gained during the cool has recovered. This value increased to 99.5% for both the second and third cycles. Although an overall modest increase (<5%) in strain is observed during the cooling, initial strain induced in the material is also small (~25%).

Conclusions

In this present contribution, we successfully synthesized well-defined POSS-initiated telechelics via ring-opening polymerization and used them to make photocured networks. Incorporation of the POSS diol, used as a difunctional initiator, at varying levels via the POSS/PCL ratio, controlled the physical properties of the telechelics and subsequent networks. The POSS content was varied from 22 to 47 wt % in the networks, giving a range of materials with competition between POSS and PCL crystallization. Higher POSS-content networks exhibited two distinct rubbery plateaus during the heating runs of tensile dynamic mechanical analysis: the first plateau at $T_{g,PCL} < T < T_{m,POSS}$, being attributed to POSS crystalline aggregates and the second at $T > T_{m,POSS}$ being due to the chemical cross-links. Further crystallization experiments led to the conclusion that POSS forms a percolating, physical network among the chemical network of the PCL chains, resulting in a chemical/physical double-network. One composition was further studied for its thermoelastic properties, revealing excellent one-way shape memory response (shape fixing and recovery) and modest two-way shape memory in the form of cooling induced elongation and heating induced contraction under constant tensile load. Future work will focus on biodegradation of the networks, the role of this degradation in dictating static mechanical and shape memory properties, and use of the materials in tissue engineering and drug delivery applications.

Acknowledgment. P.T.M. acknowledges partial support for this work by NSF under Contract DMR-0758631. The authors further thank Dr. Angel Romo-Uribe for helpful discussions.

Supporting Information Available: Figures showing (1) ^{1}H NMR spectra for (i) P-CL2.5 diol and (ii) the acrylate end-capped P-CL2.5-mac, where important peaks are indicated on the diol molecular structure, (2) optical micrograph of P-CL2 at room temperature showing spherical and rod-like aggregations of POSS along with a proposed mechanism for the self-assembly of the POSS−PCL diols, and (3) dynamic mechanical analysis for P-CL2.75-net on an expanded temperature scale. This material is available free of charge via the Internet at http://pubs.acs.org.

References and Notes

(1) Deng, Q.; Moore, R. B.; Mauritz, K. A. *J. Appl. Polym. Sci.* **1998**, *68*, 747–763.
(2) Loy, D. A. *Hybrid Mater.* **2007**, 225–254.
(3) Maiti, P.; Batt, C. A.; Giannelis, E. P. *Biomacromolecules* **2007**, *8*, 3393–3400.
(4) Xu, Y.; Brittain, W. J.; Vaia, R. A.; Price, G. *Polymer* **2006**, *47*, 4564–4570.
(5) Liu, L.; Qi, Z.; Zhu, X. *J. Appl. Polym. Sci.* **1999**, *71*, 1133–1138.
(6) Waddon, A. J.; Coughlin, E. B. *Chem. Mater.* **2003**, *15*, 4555–4561.
(7) Mather, P. T.; Jeon, H. G.; Romo-Uribe, A.; Haddad, T. S.; Lichtenhan, J. D. *Macromolecules* **1999**, *32*, 1194–1203.
(8) Romo-Uribe, A.; Mather, P. T.; Haddad, T. S.; Lichtenhan, J. D. *J. Polym. Sci., Part B: Polym. Phys.* **1998**, *36*, 1857–1872.
(9) Lichtenhan, J. D.; Otonari, Y. A.; Carr, M. J. *Macromolecules* **1995**, *28*, 8435–7.
(10) Tsuchida, A.; Bolln, C.; Sernetz, F. G.; Frey, H.; Muelhaupt, R. *Macromolecules* **1997**, *30*, 2818–2824.
(11) Mantz, R. A.; Jones, P. F.; Chaffee, K. P.; Lichtenhan, J. D.; Gilman, J. W.; Ismail, I. M. K.; Burmeister, M. J. *Chem. Mater.* **1996**, *8*, 1250−1259.
(12) Lee, A.; Lichtenhan, J. D. *Macromolecules* **1998**, *31*, 4970–4974.
(13) Hong, B.; Thoms, T. P. S.; Murfee, H. J.; Lebrun, M. J. *Inorg. Chem.* **1997**, *36*, 6146–6147.
(14) Zheng, L.; Waddon, A. J.; Farris, R. J.; Coughlin, E. B. *Macromolecules* **2002**, *35*, 2375–2379.
(15) Waddon, A. J.; Zheng, L.; Farris, R. J.; Coughlin, E. B. *Nano Lett.* **2002**, *2*, 1149–1155.
(16) Fu, B. X.; Hsiao, B. S.; White, H.; Rafailovich, M.; Mather, P. T.; Jeon, H. G.; Phillips, S.; Lichtenhan, J.; Schwab, J. *Polym. Int.* **2000**, *49*, 437–440.
(17) Fu, B. X.; Yang, L.; Somani, R. H.; Zong, S. X.; Hsiao, B. S.; Phillips, S.; Blanski, R.; Ruth, P. *J. Polym. Sci., Part B: Polym. Phys.* **2001**, *39*, 2727–2739.
(18) Kim, B.-S.; Mather, P. T. *Macromolecules* **2002**, *35*, 8378–8384.
(19) Kim, B.-S.; Mather, P. T. *Macromolecules* **2006**, *39*, 9253–9260.
(20) Matejka, L.; Strachota, A.; Plestil, J.; Whelan, P.; Steinhart, M.; Slouf, M. *Macromolecules* **2004**, *37*, 9449–9456.
(21) Kim, G. M.; Qin, H.; Fang, X.; Sun, F. C.; Mather, P. T. *J. Polym. Sci., Part B: Polym. Phys.* **2003**, *41*, 3299–3313.
(22) Zucchi, I. A.; Galante, M. J.; Williams, R. J. J.; Franchini, E.; Galy, J.; Gerard, J.-F. *Macromolecules* **2007**, *40*, 1274–1282.
(23) Bizet, S.; Galy, J.; Gerard, J.-F. *Macromolecules* **2006**, *39*, 2574–2583.
(24) Lendlein, A.; Kelch, S. *Angew. Chem., Int. Ed.* **2002**, *41*, 2034–2057.
(25) Liu, C.; Qin, H.; Mather, P. T. *J. Mater. Chem.* **2007**, *17*, 1543–1558.
(26) Jeon, H. G.; Mather, P. T.; Haddad, T. S. *Polym. Int.* **2000**, *49*, 453–457.
(27) Assfalg, N.; Finkelmann, H. *Macromol. Chem. Phys.* **2001**, *202*, 794–800.
(28) Chung, T.; Romo-Uribe, A.; Mather, P. T. *Macromolecules* **2008**, *41*, 184–192.
(29) Lendlein, A.; Schmidt, A. M.; Langer, R. *Proc. Natl. Acad. Sci. U.S.A.* **2001**, *98*, 842–7.
(30) Lendlein, A.; Schmidt, A. M.; Schroeter, M.; Langer, R. *J. Polym. Sci., Part A: Polym. Chem.* **2005**, *43*, 1369–1381.
(31) Bellin, I.; Kelch, S.; Langer, R.; Lendlein, A. *Proc. Natl. Acad. Sci. U.S.A.* **2006**, *103*, 18043–18047.
(32) Sawhney, A. S.; Pathak, C. P.; Hubbell, J. A. *Macromolecules* **1993**, *26*, 581–7.
(33) Rydholm, A. E.; Bowman, C. N.; Anseth, K. S. *Biomaterials* **2005**, *26*, 4495–4506.
(34) *Polymer Data Handbook*; Oxford University Press, Inc: Oxford, U.K., 1999.
(35) An, J. H.; Kim, H. S.; Chung, D. J.; Lee, D. S.; Kim, S. *J. Mater. Sci.* **2001**, *36*, 715–722.
(36) Fu, B. X.; Hsiao, B. S.; Pagola, S.; Stephens, P.; White, H.; Rafailovich, M.; Sokolov, J.; Mather, P. T.; Jeon, H. G.; Phillips, S.; Lichtenhan, J.; Schwab, J. *Polymer* **2001**, *42*, 599–611.
(37) Kopesky, E. T.; Haddad, T. S.; Cohen, R. E.; McKinley, G. H. *Macromolecules* **2004**, *37*, 8992–9004.
(38) Nojima, S.; Hashizume, K.; Rohadi, A.; Sasaki, S. *Polymer* **1997**, *38*, 2711–2718.
(39) Hu, H.; Dorset, D. L. *Macromolecules* **1990**, *23*, 4604–7.
(40) Wu, J.; Haddad, T. S.; Kim, G.-M.; Mather, P. T. *Macromolecules* **2007**, *40*, 544–554.
(41) Decker, C. *Macromol. Rapid Commun.* **2002**, *23*, 1067–1093.
(42) Cramer, N. B.; Bowman, C. N. *J. Polym. Sci., Part A: Polym. Chem.* **2001**, *39*, 3311–3319.

MA800586B